Carbohydrate Polymers 127 (2015) 229–235

Contents lists available at ScienceDirect

Carbohydrate Polymers

journal homepage: www.elsevier.com/locate/carbpol

Thermoset nanocomposites from waterborne bio-based epoxy resin and cellulose nanowhiskers

Guo-min Wu [a,b,*], Di Liu [a], Gui-feng Liu [a,b], Jian Chen [a], Shu-ping Huo [a], Zhen-wu Kong [a,b,*]

[a] Institute of Chemical Industry of Forest Products, Chinese Academy of Forestry, Key Laboratory of Biomass Energy and Material of Jiangsu Province, Key and Open Laboratory on Forest Chemical Engineering, State Forestry Administration, National Engineering Laboratory for Biomass Chemical Utilization, Nanjing 210042, China

[b] Research Institute of New Technology, Chinese Academy of Forestry, Beijing 10091, China

ARTICLE INFO

Article history:
Received 3 December 2014
Received in revised form 19 March 2015
Accepted 25 March 2015
Available online 3 April 2015

Keywords:
Waterborne epoxy resin
Cellulose nanowhisker
Nanocomposite
Turpentine

ABSTRACT

Thermoset nanocomposites were prepared from a waterborne terpene–maleic ester type epoxy resin (WTME) and cellulose nanowhiskers (CNWs). The curing behaviors of WTME/CNWs nanocomposites were measured with rotational rheometer. The results show that the storage modulus (G') of WTME/CNWs nanocomposites increased with the increase of CNWs content. Observations by scanning electron microscopy (SEM) demonstrate that the incorporation of CNWs in WTME matrix caused microphase separation and destroyed the compactness of the matrix. This effect leads to the glass transition temperatures (T_g) of WTME/CNWs nanocomposites slightly decrease with the increase of CNWs content, which were confirmed by both DSC and DMA tests. The mechanical properties of WTME/CNWs nanocomposites were investigated by tensile testing. The Yong's modulus (E) and tensile strength (σ_b) of the nanocomposites were significantly reinforced by the addition of CNWs. These results indicate that CNWs exhibit excellent reinforcement effect on WTME matrix, due to the formation and increase of interfacial interaction by hydrogen bonds between CNWs nano-filler and the WTME matrix.

1. Introduction

Since commercial debut in 1947, epoxy resins are widely used in coatings and adhesives because of their good adhesion for a number various materials, e.g., textiles, metals, plastics, and wood (Clayton, 1988; Sylwia, Klaudia, Ewa, Marta, & Izabela, 2013; Conradi, Kocijan, Kek-Merl, Zorko, & Verpoest, 2014; Glaris, Coulon, Dorget, & Poncin-Epaillard, 2014). Nowadays, most epoxy resin coatings are solvent based coatings. Along with the heightening sense of environment protection, coatings with low volatile organic compounds (VOCs) or without VOCs are increased rapidly. Waterborne epoxy resin coatings which offer the advantages of lower VOCs, reduced odor, decreased flammability, improved safety, and easier clean-up with water, have attracted much attention over the last several years (Li, Dai, Wan, & Zhu, 2012; Liu, Mao, Zhu, Lin, & Wang, 2013; Wan, Zang, Zhang, & Sun, 2012; Yu, Pan, & Zhou, 2014). However, unlike the homogeneous film formation of solvent-based epoxy resin coatings, the film formation of waterborne systems is a heterogeneous process among water-dispersed particles. The mechanical properties of the film of waterborne epoxy resins are not as good as that of solvent-based epoxy resin systems. It is necessary to strengthen the mechanical properties of waterborne epoxy resin coatings at the molecular level by chemical or composite modification methods.

Recently, natural fibers have been widely used as reinforcement materials in polymeric nanocomposites. CNWs also have attracted much attention as environmentally friendly nanofillers for polymer composite enhancement (Favier, Chanzy, & Cavaille, 1995; Jacob & Thomas, 2008; Eichorn et al., 2010; Klemm et al., 2011). Because of their high specific strength, modulus and aspect ratio, CNWs can significantly improve the mechanical properties of the composites at loading level as low as 5% by weight. Moreover, the advantages of CNWs stem from low density, renewable nature, biodegradability and non-toxicity. Oksman's group has performed extensive research on the production of CNWs and the processing of various polymer/CNWs nanocomposites (Bondeson, Mathew, & Oksman, 2006; Kvien, Tanem, & Oksman, 2005; Oksman, Mathew, Bondeson, & Kvien, 2006; Bondeson, Syre, & Oksman, 2007; Bondeson & Oksman, 2007a,b; Petersson, Kvien, &

* Corresponding authors at: Chinese Academy of Forestry, Institute of Chemical Industry of Forest Products, No 16, Suojin Wucun, Nanjing 210042, China. Tel.: +86 02585482457.
E-mail addresses: woogm@hotmail.com (G.-m. Wu), kongzwlhs@163.com (Z.-w. Kong).

http://dx.doi.org/10.1016/j.carbpol.2015.03.078
0144-8617/

Oksman, 2007). To realize property improvements, CNWs must be homogeneously dispersed in the polymeric matrix. However, given the high surface area, hydrophilic nature and agglomeration of the whiskers, homogeneous dispersion of the whiskers posed a great challenge in CNWs nanocomposite processing. One method to overcome this problem would be to chemically modify the surface of the CNWs by appropriate functions to enhance their interaction with the matrix (Cetin et al., 2009; Stenstad, Andresen, Tanem, & Stenius, 2008; Siqueira, Bras, & Dufresne, 2010). But the chemical strategies of surface modification of CNWs are quite inefficient. An efficient strategy for the utilization of CNWs to prepare nanocomposites without modification is to incorporate CNWs in waterborne polymers, since stable suspensions of CNWs can be easily prepared in water. So far, CNWs have been reported to be filled into thermoplastic waterborne polyurethanes, polyoxyethylenes, resulting in a significant increase of strength and Yong's modulus (Zou et al., 2011; Lee & Kim, 2012; Oliveira Patricio et al., 2013).

Waterborne epoxy resin is an ideal waterborne matrix. It has high level of compatibility with water-dispersible CNWs, and therefore reduces or eliminates the need for chemical modification of CNWs. Only two studies have been conducted for CNWs composites with a waterborne epoxy resin, using waterborne epoxy resin derived from bisphenol-A (BPA) (Matos Ruiz, Cavaille, Dufresne, Gerard, & Graillat, 2000; Xu, Girouard, Schueneman, Shofner, & Carson Meredith, 2013). However, BPA is a fossil oil based chemical and may mimic the body's own hormones and may lead to several negative health effects (Gore, 2007; Vandenberg, Hunt, Myers, & Vom Saal, 2013; Okada et al., 2008; Vom Saal, Nagel, Coe, Angle, & Taylor, 2012). The negative impact of BPA on human health necessarily implies the elimination of BPA, especially since some countries, such as Canada or France, have recently banned the use of BPA in food contact materials (Guo, 2012). In our previous work, a biomass based epoxy resin (denoted as TME) and a waterborne dispersion of TME (denoted as WTME) were prepared from the raw material turpentine which is a common biomass material in China (Wu, Kong, Huang, Chen, & Chu, 2007; Liu, Huang, Kong, Wu, & Chen, 2009a,b). TME and WTME are non-toxic alicyclic structure epoxy resins without BPA. But the mechanical properties of cured products of them were not as good as those of BPA based epoxy resin. In this work, we incorporated with CNWs suspension, which were hydrolyzed from microcrystalline cellulose (MCC), into the above WTME to prepare novel biomass based thermoset nanocomposites. The curing reaction, structure and properties of resultant nanocomposites were investigated by rotational rheometer, transmission electron microscopy (TEM), scanning electron microscopy (SEM), differential scanning calorimetry (DSC), thermogravmetric analysis (TGA), dynamic mechanical analysis (DMA), and tensile tests.

2. Experimental

2.1. Materials

Terpene–maleic ester type epoxy resin (TME) with endocyclic structure (Fig. 1) and epoxy value of 3.5 mmol g^{-1} was synthesized from turpentine (Wu et al., 2007). TME based emulsifier (Fig. 1) was prepared with TME and polyethylene glycol (PEG) (Liu et al., 2009a,b). Polyethylene glycol (M_n = 4000) was obtained from Guangdong Xilong Chemical Co., Ltd., China. Microcrystalline cellulose (MCC) was purchased from Aladdin Industrial Co., China. Sulfuric acid (H_2SO_4) was purchased from Sinopharm Chemical Reagent Co., Ltd., China. The hydrophilically modified aliphatic amine curing agent (Fig. 1) with amine value of 115 mg g^{-1} and solid content of 45 wt%, was supplied by Zhejiang Anbang New Material Development Co., Ltd., China.

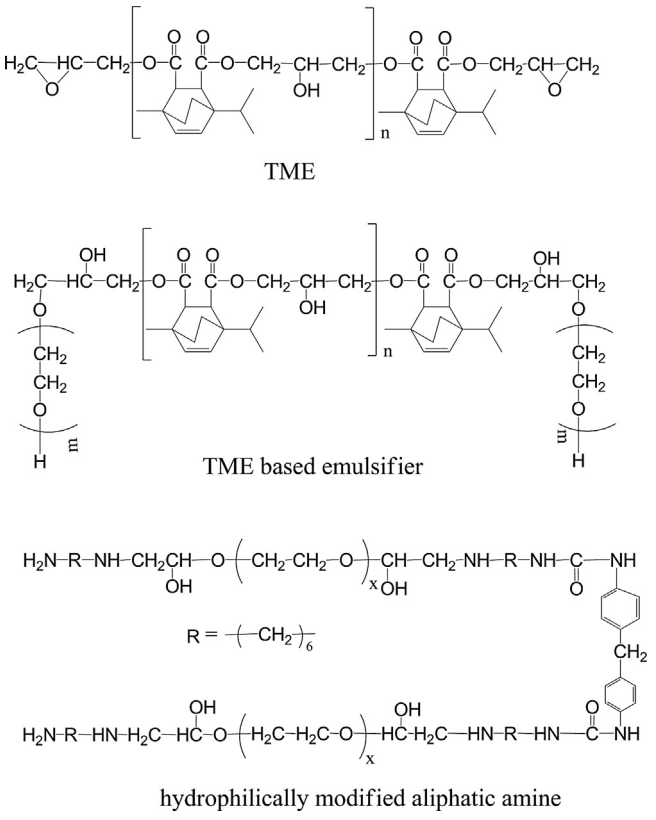

Fig. 1. Chemical structures of TME, TME based emulsifier and the aliphatic amine.

2.2. Preparation of TME based emulsifier

TME based emulsifier was prepared according to our previous work (Liu et al., 2009a,b). A 500 ml four-necked flask equipped with stirrer, dropping funnel, thermometer and condenser was charged with 15 g TME and 216 g polyethylene glycol (M_n = 4000). After TME and polyethylene glycol were mixed homogeneously by constant stirring at 90 °C, 1.15 g boron fluoride ethyl ether was added to the reaction system as catalyst. The reaction was continued for 1 h at 110 °C, and a yellow transparent product (TME based emulsifier) was obtained.

2.3. Preparation of WTME

The preparation of WTME was described in our previous work (Liu et al., 2009a,b). A 1000 ml four-necked flask equipped with stirrer, dropping funnel, thermometer and condenser was charged with 200 g TME and 40 g TME based emulsifier. After TME and TME based emulsifier were mixed homogeneously by constant stirring at 60 °C and a stirring speed of 800 r min^{-1} for 30 min, the system was cooled to ambient temperature (25 °C). Then distilled water was continuously added to drive the phase inversion at ambient temperature. When the conductivity of the system increased abruptly, phase inversion occurred and the concentrated WTME dispersion was prepared. Water was further added in order to dilute the concentrated dispersion. Then a milk-white dispersion (WTME dispersion) with 40 wt.% solid content was obtained. The micro-morphology of the particles of WTME dispersion collected with a transmission electron microscopy (TEM) is shown in Fig. 2(a). The diameters of WTME particles range from 50 nm to 200 nm.

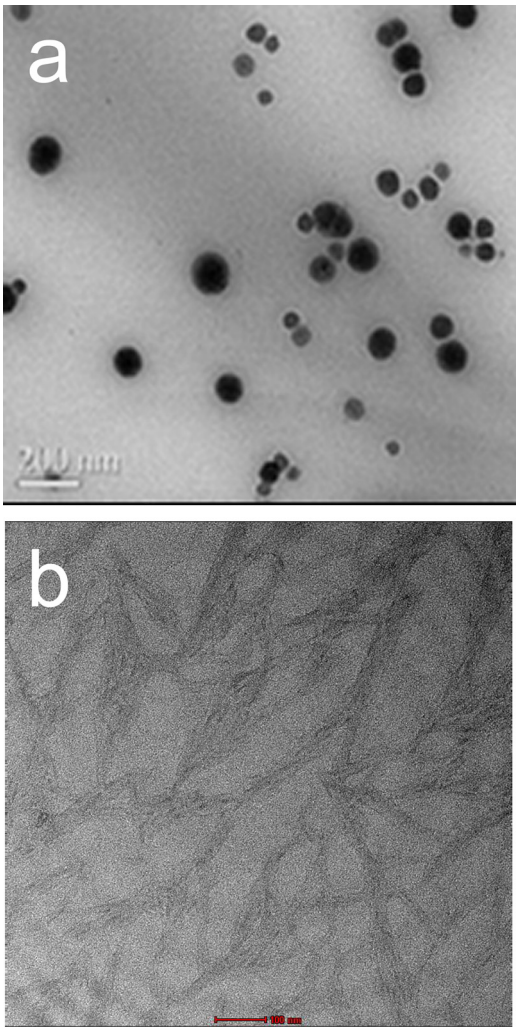

Fig. 2. TEM images of WTME and CNWs.

2.4. Preparation of CNWs

According to the previous report (Bondeson et al., 2006), 10.0 g MCC and 110 ml sulfuric acid solution (63.5 wt%) were put into a 500 ml three-necked flask and stirred vigorously for 2 h at 44 °C. A water/CNWs suspension was obtained after diluted with 500 g distilled water to stop the reaction. The suspension was then centrifuged and washed with distilled water repeatedly. The last wash was conducted using dialysis with distilled water. After concentrated under vacuum and adjusted with distilled water, a stable suspension with CNWs content of 3.0 wt% was obtained through 30 min ultrasonic treatment. The stereoscopic information of the CNWs collected with TEM is shown in Fig. 2(b). The rod-like CNWs were observed having the width of 20–40 nm and the length of 200–400 nm.

2.5. Preparation of WTME/CNWs nanocomposite films

The WTME dispersion was mixed with CNWs suspension under the condition of sonication for 10 min. Then the mixture was further blended with the hydrophilically modified aliphatic amine curing agent in the molar ratio of epoxy group to active hydrogen group 1:1. The resulting blend called WTME/CNWs dispersion was diluted with distilled water to the solid content of 30 wt%, and then degassed under vacuum at ambient temperature. Subsequently, the WTME/CNWs dispersion was cast in a square Teflon molds and dried at 30 °C for 1 week. By altering the content of CNWs in the range of 0, 0.5, 1, 2, 4, 8 wt% in relation to solid resin (WTME and aliphatic amine curing agent), a series of nanocomposite films with a thickness of approximately 0.5 mm were obtained, and denoted as 0 wt%, 0.5 wt%, 1 wt%, 2 wt%, 4 wt%, and 8 wt%, respectively.

2.6. Characterizations

A few drops of diluted WTEM dispersion or CNWs suspension were dripped on a C-coated Cu grid, and dried under vacuum for 12 h for transmission electron microscopy (TEM) measurement. A Tecnai G2 20 S-TWIN transmission electron microscopy (FEI, USA) was used to observe the particle size and morphology of WTEM dispersion and CNWs.

The curing behaviors of WTME/CNWs were performed with the Haake Mars-III rotational rheometer (Thermo Scientific, Germany) with a cone-plate geometry (diameter of 25 mm, gap of 0.5 mm). Oscillatory measurement which allowed for the monitoring of viscoelastic properties during the curing process of WTME/CNWs was performed with a temperature sweep range of 20 °C to 150 °C at a rate of 2 K min^{-1} and at 150 °C for 30 min. The oscillation frequency was 2 Hz.

A Hitach S3400 N scanning electron microscopy (Japan) was used to observe the cross-section micrographs of the nanocomposite films at 15 kV. The films were frozen in liquid nitrogen and snapped immediately.

A PerkinElmer Diamond differential scanning calorimeter (USA) was used to perform DSC analysis of the nanocomposite films at heating rate of 20 K min^{-1} and nitrogen gas flow of 20 ml min^{-1}. The specimens were crimple-sealed in aluminum crucibles and scanned from −50 °C to 150 °C.

A NETZSCH STA 409 PC/PG thermogravimetric analyzer (Germany) was used to determine the thermal stability of the nanocomposite films. The samples were placed in an aluminum pan and heated in nitrogen atmosphere from 25°C to 600 °C at heating rate of 10 K min^{-1}.

DMA was carried out on a Q800 dynamic mechanical analyzer (TA instrument, USA) at a frequency of 1 Hz, temperature range of −50 °C to 150 °C, and heating rate of 2 K min^{-1}. The size of the specimens cut from the nanocomposite films was $40 \times 6.5 \times 0.5\ mm^3$.

A universal testing machine (CMT4304, Shenzhen SANS, China) was used to measure the tensile properties of the nanocomposite films at loading rate of 100 mm min^{-1} according to the standard ASTM D412 at room temperature. An average value of five replicates for each specimen was taken.

3. Results and discussion

3.1. Curing process of WTME/CNWs dispersions

Fig. 3 shows the storage modulus (G') variation during the curing process of WTME/CNWs with different CNWs contents. At the beginning of the temperature-rise period, the viscosities of WTME/CNWs decrease with the temperature increase, leading to a fall of G'. With the increase of temperature, the curing reaction between epoxy groups and amine groups takes place, leading to a fast increase of G'. During the period of constant temperature at 150 °C, G' increases slowly and some G' values keep roughly stable afterwards, indicating the curing of the reactions is almost accomplished. When the temperature decreases, the WTME/CNWs nanocomposite gradually changes from a rubbery state to a glassy state, leading to a rapidly growth of G'. Compared to neat WTME (0 wt%), all the WTME/CNWs nanocomposites show significant enhancement of G'. At the end of the reaction, the increase of G' is proportional to the CNWs loading level in the range of 0–8 wt%.

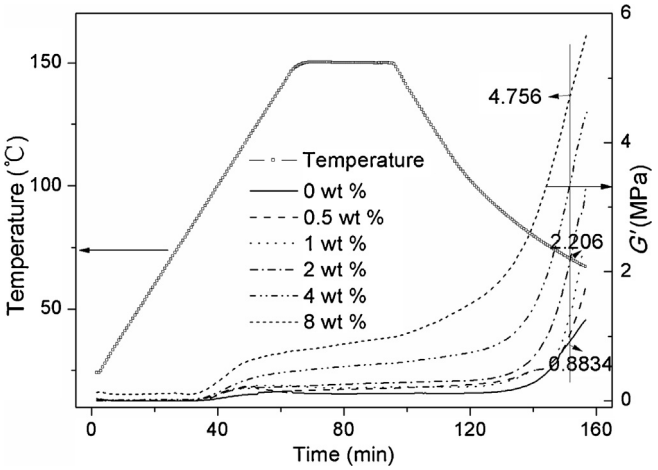

Fig. 3. Variation of the storage modulus (G') during the curing process of WTME/CNWs.

As shown in Fig. 3, for the WTME/CNWs nanocomposite containing 2 wt% and 8 wt%, G' is about 150% and 438%, respectively, higher than that of the neat WTME (0 wt%) at the same temperature 70 °C. The simultaneous enhancement of G' can be attributed to the well homodispersion of the CNWs in nano-scale (Chen et al., 2008) as well as the formation and increase of physical interaction by hydrogen bonds between CNWs nano-filler and the WTME matrix.

3.2. Morphology of WTME/CNWs nanocomposite films

The micromorphologies of the fractured surfaces of WTME/CNWs nanocomposite films are shown in Fig. 4. Compared to the micrograph of the neat WTME (0 wt%), the fractured surfaces of WTME/CNWs nanocomposite films become more rough, and more "sea-island structure" appear in the micromorphology of WTME/CNWs nanocomposite films with the increase of CNWs content. The formation of "sea-island structure" could correspond to the microphase separation between the CNWs nano-filler and the WTME matrix, which indicates a more complicated energy dissipating mechanism with the interfaces between CNWs and the WTME matrix (Gao et al., 2012), and results in the variation of the properties of the nanocomposite films. The "sea-island structure" uniform distribution all over the fractured surface indicates the well dispersion of CNWs in the WTME. The compatibility of the interfaces between the nano-fillers and matrix can be enhanced by the interactions from hydrogen bonds between the surface hydroxyl groups of CNWs and the polar groups of WTME matrix. However, as shown in Fig. 4, adding CNWs to WTME polymer would destroy the compactness of the matrix.

Table 1
Thermal properties of WTME/CNWs nanocomposite films.

Sample (CNWs content) (wt%)	T_g (°C)	$T_{5\%}$ (°C)
0	47.8	242.3
0.5	46.7	245.7
1	45.5	246.0
2	44.8	244.9
4	43.8	243.4
8	43.1	240.3

3.3. DSC analysis of WTME/CNWs nanocomposite films

The glass transition temperatures (T_g) of the WTME/CNWs nanocomposite films were measured by DSC analysis. Fig. 5 shows the DSC thermograms of WTME/CNWs nanocomposites with different CNWs contents. The data showing Fig. 5 are listed in Table 1. The T_g of the nanocomposites shifts toward lower temperature with the increase of CNWs content. Change of CNWs contents from 0 to 8 wt% results in the decrease of T_g from 48.3 °C to 43.1 °C. This result is opposite to our previous research about incorporating CNWs into the biomass-based two-component waterborne polyurethanes (2K-WPU) (Wu, Chen, Huo, Liu, & Kong, 2014). In the 2K-WPU/CNWs system, the active hydroxyl groups on the surface

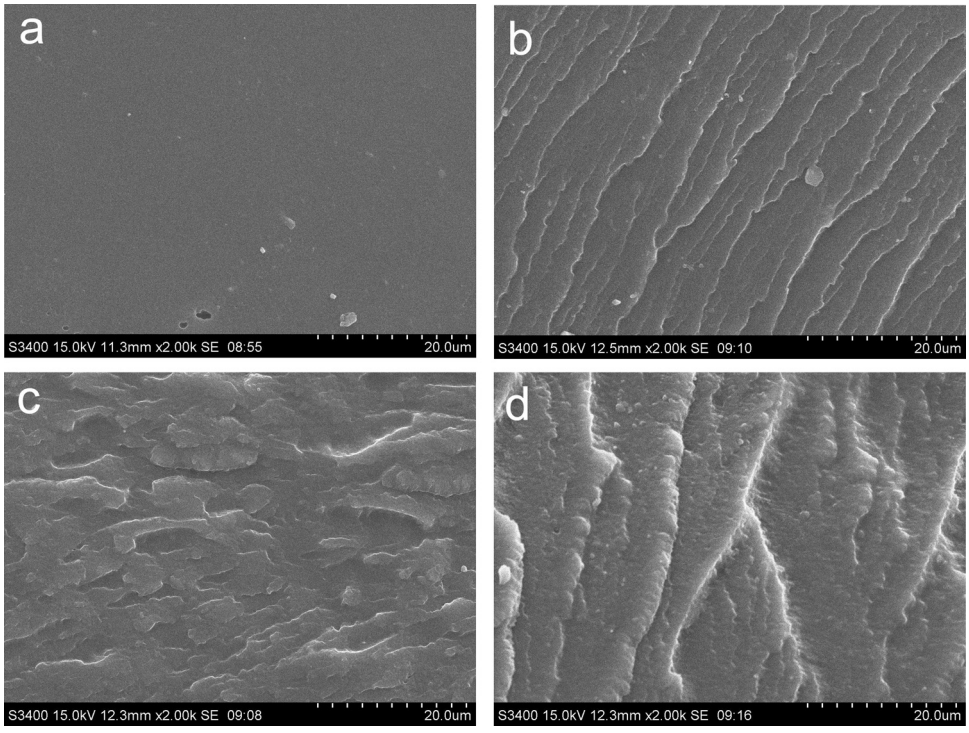

Fig. 4. SEM images of WTME/CNWs nanocomposite films with different CNWs contents (a) 0 wt%; (b) 2 wt%; (c) 4 wt%; (d) 8 wt% (scale bar: 20 μm).

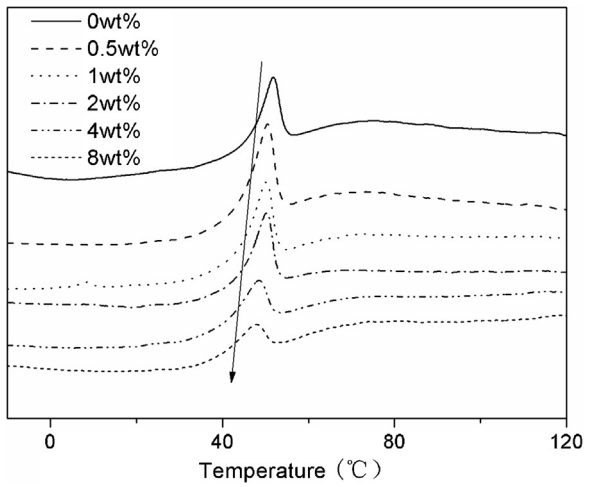

Fig. 5. DSC thermograms of WTME/CNWs nanocomposite films with different CNWs loading level.

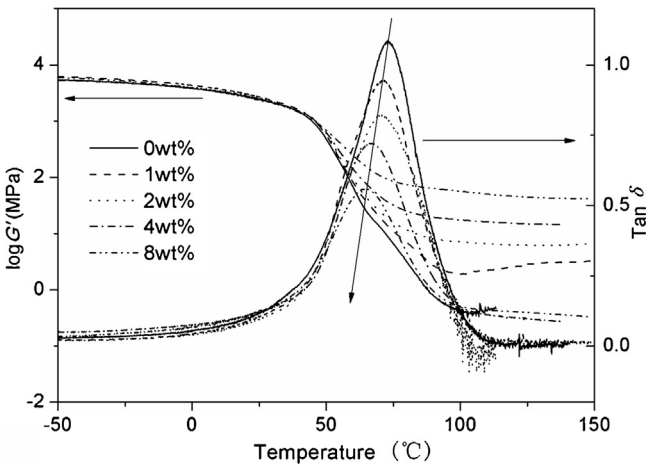

Fig. 7. DMA curves of WTME/CNWs nanocomposite films with different CNWs contents.

of CNWs can take part in the crosslinking reaction with isocyanate groups of 2K-WPU, resulting in strong interfacial adhesion between the 2K-WPU matrix and CNWs. A rigid CNWs nano-phase plays a role as another type of crosslinking points in the 2K-WPU matrix. As a result, the motion of polymer chains can be suppressed by the rigid CNWs nano-phase, which leads to T_g shift to high temperature. However, in the WTME/CNWs nanocomposite, there are only hydrogen bonds formed between CNWs and the WTME matrix. The interfacial adhesion of hydrogen bonds is not as strong as that of chemical grafting. Moreover, as shown in Fig. 4, adding CNWs into WTME polymer expands the free volume of the nanocomposite at the interface between CNWs and the matrix, which can also result in the shift of T_g toward lower values.

3.4. Thermogravmetric analysis of WTME/CNWs nanocomposite films

The TGA and the DTG curves of neat WTME (0 wt%), WTME/CNWs nanocomposites with different CNWs contents, and CNWs powder are shown in Fig. 6. There are two weight loss stages observed in the TGA curve of neat WTME. The first weight loss peak occurs at about 300 °C, corresponding to the degradation of aliphatic amine curing agent due to its low breaking energy of C—N bond. The second peak at about 405 °C is attributed to the

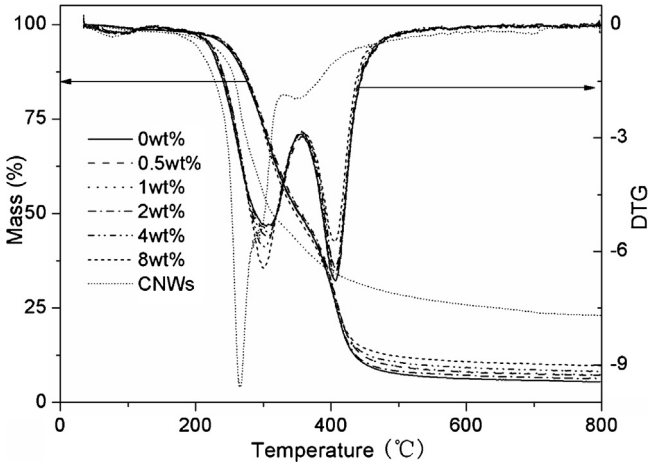

Fig. 6. TGA and DTG curves of WTME/CNWs nanocomposites with different CNWs contents and CNWs.

decomposition of WTME. The TGA curve of CNWs shows a typical degradation of CNWs possessing sulfate groups which arose from fiber hydrolysis with sulfuric acid (Roman & Winter, 2004; Cao, Habibi, & Lucia, 2009). Compared to the TGA curves of CNWs and neat WTME, the thermograms of WTME/CNWs nanocomposites with different CNWs contents are similar to that of neat WTME. No separate degradation stage of CNWs can be observed in any TGA thermogram of WTME/CNWs nanocomposites regardless of CNWs loading level. This indicates that CNWs have been trapped in the cross-linked network of WTME and completely covered by polymer chains through hydrogen bonds. The thermal degradation temperatures of 5% weight loss ($T_{5\%}$) are listed in Table 1. $T_{5\%}$ of WTME/CNWs nanocomposites is found to first slightly increase and then decrease with the increase of CNWs content. The possible explanation of this phenomenon is that the addition of CNWs results in a complicated energy dissipating mechanism of the interfaces between CNWs and the WTME matrix, and causes an increase of thermal conductivity of the material (Shimazaki et al., 2007).

3.5. DMA analysis of WTME/CNWs nanocomposite films

Fig. 7 shows the dynamic mechanical properties including the storage modulus (G') and the loss factor (tan δ) of WTME/CNWs nanocomposite films with different CNWs contents. The α-relaxation temperature (T_α), temperature at which tan δ passed through the maximum, corresponds to the main mechanical relaxation associated with the glass transition of the polymers. As shown in Fig. 7, T_α of the WTME/CNWs nanocomposites shifts toward lower temperature, and the intensity of tan δ peaks decreases with the increase of CNWs content. These results are in agreement with the T_g tests from DSC (Table 1). The decrease of tan δ peaks intensity suggests that the energy dissipation process is slowed down by the nano-fillers (Chen et al., 2008). The decrease of T_α of the WTME/CNWs nanocomposites suggests that the microphase separation and the compactness destruction of the matrix are more prominent with the increase of CNWs content. Variation trends of the storage modulus (G') curves of WTME/CNWs nanocomposites with different CNWs contents are similar to that of the neat WTME. At low temperature (below 0 °C), the matrix is in the glassy state and G' remains roughly constant. A rapid decrease of G' is observed when the temperature is close to T_α, corresponding to the glass transition. At the temperature above T_α, the G' values of WTME/CNWs nanocomposites increase significantly with the increase of CNWs content, which is in good agreement with the results obtained by rotational rheometer measurements. The

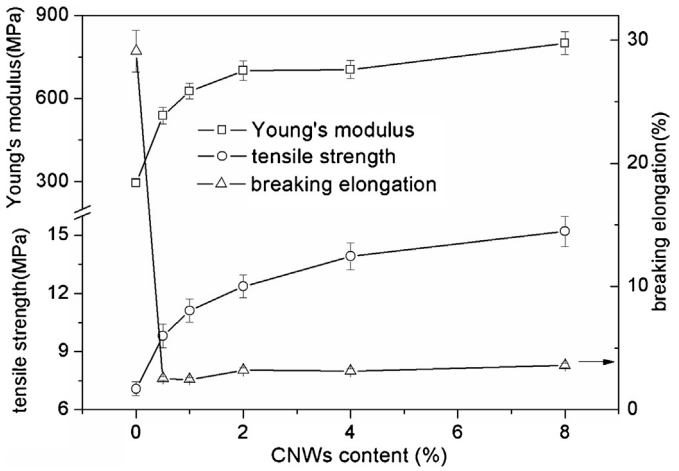

Fig. 8. Effects of CNWs content on Yong's modulus (E), tensile strength (σ_b) and break elongation (ε_b) of WTME/CNWs nanocomposite films.

Table 2
Tensile properties of WTME/CNWs nanocomposite films.

Sample (CNWs content) (wt%)		E (MPa)	σ_b (MPa)	ε_b (%)
0	Average value	295.6	7.08	29.11
	Standard deviation	12.37	0.358	1.702
0.5	Average value	538.3	9.81	2.54
	Standard deviation	29.72	0.606	0.136
1	Average value	626.2	11.11	2.46
	Standard deviation	28.56	0.601	0.141
2	Average value	700.5	12.37	3.21
	Standard deviation	35.48	0.593	0.206
4	Average value	704.6	13.92	3.14
	Standard deviation	33.06	0.698	0.207
8	Average value	800.1	15.2	3.61
	Standard deviation	41.56	0.781	0.195

enhancement of G' is attributed to the well homodispersion of the CNWs in nano-scale as well as the formation and increase of interfacial interaction by hydrogen bonds between CNWs nano-filler and the WTME matrix. However, at the low temperature when the matrix is in the glassy state, the enhancement of G' of the WTME by adding CNWs is not clear. On the one hand, the motions of the chains are largely restricted in the glassy state, therefore it is difficult and indistinct to further restrain the motion with CNWs. On the other, the accurate determination of the glassy modulus is difficult because of its dependence on the sample dimensions (Matos Ruiz et al., 2000).

3.6. Tensile properties of WTME/CNWs nanocomposite films

Fig. 8 shows the tensile properties of WTME/CNWs nanocomposite films with different CNWs contents, measured at room temperature (about 25 °C). The data including Yong's modulus (E), tensile strength (σ_b), and break elongation (ε_b) are summarized in Table 2. Compared with neat WTME, all the nanocomposites show simultaneous enhancement in E and σ_b with the increase of CNWs content. E and σ_b of WTME/CNWs nanocomposite containing 8 wt% CNWs are about 171% and 115%, respectively, higher than those of neat WTME. The modulus enhancement can be attributed to the restrained chain movement during the tensile deformation due to the existence of CNWs. And the improvement of tensile strength is attributed to the formation and increase of interfacial interaction by hydrogen bonds between CNWs and the WTME matrix with an increase of CNWs content (Ten, Turtle, Bahr, Jiang, & Wolcott, 2010). However, break elongation of WTME/CNWs nanocomposite films decreases with the increase of CNWs content. The fractography images of WTME/CNWs nanocomposite films are shown in Fig. 4. The decrease of elongation can be attributed to the decrease of polymer extensibility, which is caused by the formation of a rigid CNWs nano-phase (the "sea-island structure" in the fractography images in Fig. 4) and by the microphase separation between the CNWs nano-filler and the WTME matrix.

4. Conclusion

New thermoset matrix nanocomposites with well dispersed of CNWs have been prepared by adding CNWs in a waterborne biomass based epoxy resin (WTME). The incorporation of CNWs in WTME matrix (0.5–8 wt%) increased the storage modulus (G'), Yong's modulus (E) and tensile strength (σ_b) as revealed by rotational rheometer measurements, DMA, and tensile tests, indicating good reinforcement of the epoxy resin matrix. These effects are attributed to the formation and increase of interfacial interaction by hydrogen bonds between CNWs nano-filler and the WTME matrix. DSC and TGA analyses show incorporating CNWs into WTME matrix slight affects the glass transition (T_g) and the thermal stability of the nanocomposites. These results are due to the microphase separation between the CNWs nano-filler and the WTME matrix causing a complicated energy dissipating mechanism of the materials. All the variations of the properties of WTME/CNWs nanocomposites are caused by the incorporation of rigid CNWs nano-phase in WTME matrix and the formation of hydrogen bonds between CNWs nano-filler and the WTME matrix.

Conflict of interest statement

The authors have no conflicts of interest to declare.

Acknowledgement

The authors gratefully acknowledge the financial support from the National Natural Science Foundation of China (contract grant number: 31100428).

References

Bondeson, D., Mathew, A. P., & Oksman, K. (2006). Optimization of the isolation of nanocrystals from microcrystalline cellulose by acid hydrolysis. *Cellulose*, *13*, 171–180.

Bondeson, D., & Oksman, K. (2007a). Polylactic acid/cellulose whisker nanocomposites modified by polyvinyl alcohol. *Composites A: Applied Science and Manufacturing*, *38*, 2486–2492.

Bondeson, D., & Oksman, K. (2007b). Dispersion and characteristics of surfactant modified cellulose whiskers nanocomposites. *Composite Interfaces*, *14*, 617–630.

Bondeson, D., Syre, P., & Oksman, K. (2007). All cellulose nanocomposites produced by extrusion. *Journal of Biomaterials and Bioenergy*, *1*, 367–371.

Cao, X. D., Habibi, Y., & Lucia, L. A. (2009). One-pot polymerization, surface grafting, and processing of waterborne polyurethane-cellulose nanocrystal nanocomposites. *Journal of Materials Chemistry*, *19*, 7137–7145.

Cetin, N. S., Tingaut, P., Ozmen, N., Henry, N., Harper, D., Dadmun, M., et al. (2009). The acetylation of cellulose nanowhiskers with vinyl acetate under moderate conditions. *Macromolecular Bioscience*, *9*, 997–1003.

Chen, G. J., Wei, M., Chen, J. H., Huang, J., Dufresne, A., & Chang, P. R. (2008). Simultaneous reinforcing and toughening: New nanocomposites of waterborne polyurethane filled with low loading level of starch nanocrystals. *Polymer*, *49*, 1860–1870.

Clayton, M. (1988). *Epoxy resins: Chemistry and technology* (2nd ed.). Marcel Dekker: New York, NY.

Conradi, M., Kocijan, A., Kek-Merl, D., Zorko, M., & Verpoest, I. (2014). Mechanical and anticorrosion properties of nanosilica-filled epoxy-resin composite coatings. *Applied Surface Science*, *292*, 432–437.

Eichorn, S. J., Dufresne, A., Aranguren, M., Marcovitch, N. E., Capadona, J. R., Rowan, S. J., et al. (2010). Review: Current international research into cellulose nanofibres and nanocomposites. *Journal of Materials Science*, *45*, 1–33.

Favier, V., Chanzy, H., & Cavaille, J. Y. (1995). Polymer nanocomposites reinforced by cellulose whiskers. *Macromolecules*, *28*, 6365–6367.

Gao, Z. Z., Peng, J., Zhong, T. H., Sun, J., Wang, X. B., & Yue, C. (2012). Biocompatible elastomer of waterborne polyurethane based on castor oil and polyethylene glycol with cellulose nanocrystals. *Carbohydrate Polymers*, *87*, 2068–2075.

Glaris, P., Coulon, J. F., Dorget, M., & Poncin-Epaillard, F. (2014). Fluorinated epoxy resin as a low adhesive mould for composite material. *Composites B: Engineering*, *63*, 94–100.

Gore, A. C. (2007). *Endocrine disturbing chemicals: From basic research to clinical practice*. Totowa, NJ: Humana Press.

Guo, Y. M. (2012). Analysis of health hazards, legal restrictions and regulations for BPA. *Modern Food Science & Technology*, *5*, 549–551.

Jacob, M., & Thomas, S. (2008). Review: Biofibres and biocomposites. *Carbohydrate Polymers*, *71*, 353–364.

Klemm, D., Kramer, F., Moritz, S., Lindstrom, T., Ankerfors, M., Gray, D., et al. (2011). Nanocelluloses: A new family of nature-based materials. *Angewandte Chemie*, *50*, 5438–5466.

Kvien, I., Tanem, B. S., & Oksman, K. (2005). Characterization of cellulose whiskers and their nanocomposites by atomic force and electron microscopy. *Biomacromolecules*, *6*, 3160–3165.

Lee, S. J., & Kim, B. K. (2012). Covalent incorporation of starch derivative into waterborne polyurethane for biodegradability. *Carbohydrate Polymers*, *87*, 1803–1809.

Li, Y. Y., Dai, H. Q., Wan, L., & Zhu, Z. J. (2012). Surface sizing application of waterborne epoxy resin on low basis weight paper. *BioResources*, *7*, 5–14.

Liu, M., Mao, X. H., Zhu, H., Lin, A., & Wang, D. H. (2013). Water and corrosion resistance of epoxy–acrylic–amine waterborne coatings: Effects of resin molecular weight, polar group and hydrophobic segment. *Corrosion Science*, *75*, 106–113.

Liu, Y., Huang, H., Kong, Z. W., Wu, G. M., & Chen, J. (2009a). Preparation and characteristics of non-ionic waterborne emulsifier from terpinene–maleic ester type epoxy resin. *Chemistry & Industry of Forest Products*, *29*, 23–29.

Liu, Y., Huang, H., Kong, Z. W., Wu, G. M., & Chen, J. (2009b). Preparation and properties of water-emulsified terpinene–maleic ester type epoxy resin by phase-inversion emulsification. *Chemistry & Industry of Forest Products*, *29*, 18–24.

Matos Ruiz, M., Cavaille, J. Y., Dufresne, A., Gerard, J. F., & Graillat, C. (2000). Processing and characterization of new thermoset nanocomposites based on cellulose whiskers. *Composite Interfaces*, *7*, 117–131.

Okada, H., Tokunaga, T., Liu, X., Takayanagi, S., Matsushima, A., & Shimohigashi, Y. (2008). Direct evidence revealing structural elements essential for the high binding ability of bisphenol A to human estrogen-related receptor-gamma. *Environmental Health Perspectives*, *116*, 32–38.

Oksman, K., Mathew, A. P., Bondeson, D., & Kvien, I. (2006). Manufacturing process of polylactic acid (PLA)–cellulose whiskers nanocomposites. *Composite Science and Technology*, *66*, 2776–2784.

Oliveira Patricio, P. S., Miranda, I. P., Silva, N. C. F., Ayres, E., Pereira, F. V., & Orefice, R. L. (2013). Tailoring the morphology and properties of waterborne polyurethanes by the procedure of cellulose nanocrystal incorporation. *European Polymer Journal*, *49*, 3761–3769.

Petersson, L., Kvien, I., & Oksman, K. (2007). Structure and thermal properties of poly(lactic acid)/cellulose whiskers nanocomposites. *Composite Science and Technology*, *67*, 2535–2544.

Roman, M., & Winter, W. T. (2004). Effect of sulfate groups from sulfuric acid hydrolysis on the thermal degradation behavior of bacterial cellulose. *Biomacromolecules*, *5*, 1671–1677.

Shimazaki, Y., Miyazaki, Y., Takezawa Masaya Nogi, M., Abe, K., Ifuku, S., & Hiroyuki Yano, H. (2007). Excellent thermal conductivity of transparent cellulose nanofiber/epoxy resin nanocomposites. *Biomacromolecules*, *8*, 2976–2978.

Siqueira, G., Bras, J., & Dufresne, A. (2010). New process of chemical grafting of cellulose nanoparticles with a long chain isocyanate. *Langmuir*, *26*, 402–411.

Stenstad, P., Andresen, M., Tanem, B. S., & Stenius, P. (2008). Chemical surface modifications of microfibrillated cellulose. *Cellulose*, *15*, 35–45.

Sylwia, W., Klaudia, Z., Ewa, L., Marta, L., & Izabela, G. (2013). Organic coatings based on new Schiff base epoxy resins. *Progress in Organic Coatings*, *76*, 1040–1045.

Ten, E., Turtle, J., Bahr, D., Jiang, L., & Wolcott, M. (2010). Thermal and mechanical properties of poly(3-hydroxybutyrate-*co*-3-hydroxyvalerate)/cellulose nanowhiskers composites. *Polymer*, *51*, 2652–2660.

Vandenberg, L. N., Hunt, P. A., Myers, J. P., & Vom Saal, F. S. (2013). Human exposures to bisphenol A: Mismatches between data and assumptions. *Reviews on Environmental Health*, *28*, 37–58.

Vom Saal, F. S., Nagel, S. C., Coe, B. L., Angle, B. M., & Taylor, J. A. (2012). The estrogenic endocrine disrupting chemical bisphenol A (BPA) and obesity. *Molecular and Cellular Endocrinology*, *354*, 74–84.

Wan, T., Zang, T. S., Zhang, R., & Sun, X. C. (2012). Cure behaviors and water uptake evaluation of a new waterborne epoxy resin. *Journal of Wuhan University of Technology—Materials Science Edition*, *27*, 437–442.

Wu, G. M., Chen, J., Huo, S. P., Liu, G. F., & Kong, Z. W. (2014). Thermoset nanocomposites from two-component waterborne polyurethanes and cellulose whiskers. *Carbohydrate Polymers*, *105*, 207–213.

Wu, G. M., Kong, Z. W., Huang, H., Chen, J., & Chu, F. X. (2007). Synthesis of epoxy resin from hydrogenated terpinene–maleic anhydride. *Chemistry & Industry of Forest Products*, *27*, 57–62.

Xu, S. H., Girouard, N., Schueneman, G., Shofner, M. L., & Carson Meredith, J. (2013). Mechanical and thermal properties of waterborne epoxy composites containing cellulose nanocrystals. *Polymer*, *54*, 6589–6598.

Yu, J. F., Pan, H. X., & Zhou, X. D. (2014). Preparation of waterborne phosphated acrylate–epoxy hybrid dispersions and their application as coil coating primer. *Journal of Coatings Technology and Research*, *11*, 361–369.

Zou, J. W., Zhang, F., Huang, J., Chang, P. R., Su, Z. M., & Yu, J. H. (2011). Effects of starch nanocrystals on structure and properties of waterborne polyurethane-based composites. *Carbohydrate Polymers*, *85*, 824–831.